IJE TRANSACTIONS A: Basics Vol. 35, No. 05, (July 2022) 1268-1282

International Journal of Engineering

Journal Homepage: www.ije.ir

Location Sensitivity of Non-structural Component for Channel-type Auxiliary Building Considering Primary-secondary Structure Interaction

M. M. Rahman[a,b], T. T. Nahar[b], D. Kim*[c], D. W. Park[a]

[a] *Department of Civil and Environmental Engineering, Kunsan National University, 558 Daehak-ro, Gunsan-si, Jeollabukdo 54150, Republic of Korea*
[b] *Department of Civil Engineering, Pabna University of Science and Technology, Rajapur, Pabna 6600, Bangladesh*
[c] *Department of Civil and Environmental Engineering, Kongju National University, 1223-24 Cheonan-daero, Seobuk-gu, Cheonan, Chungcheongnam-do 31080, Republic of Korea*

PAPER INFO

Paper history:
Received 05 February 2022
Received in revised form 05 March 2022
Accepted 09 March 2022

Keywords:
Non-structural Components
Auxiliary Building
Zero-period Acceleration
Seismic Response
Primary-secondary Structure Interaction
Response Surface Methodology

ABSTRACT

To ensure the safe and stable operation of nuclear power plants (NPP), many non-structural components (NSCs) are actively associated with NPP. Generally, floor response spectrum (FRS) is used to design the NSCs. Nevertheless, it is essential to focus on the mounting position and frequency of NSCs which is normally ignored during the conventional design of NSCs. This paper evaluates the effect of mounting location for NSCs over the same floor in a channel-type auxiliary building. The modal parameter estimation is taken into account to capture the dynamic property of the NPP auxiliary building by the shake table test; which leads to the calibration of the finite element model (FEM). The calibration of FEM was conducted through response surface methodology (RSM) and the calibrated model is verified utilizing modal parameters as well as frequency response spectrum function. Finally, the location sensitivity was investigated by time history analysis (THA) under artificially generated design response spectrum compatible earthquakes and sine sweeps. The result showed that the right choice of location for NSCs can be an important measure to reduce the undesirable responses during earthquakes, which can reduce up to 30% horizontal and 70% vertical zero period acceleration (ZPA) responses in channel-type auxiliary buildings.

doi: *10.5829/ije.2022.35.07a.06*

1. INTRODUCTION

Earthquake (EQ) is a natural hazard and loads due to EQ have the greatest influence on nuclear power plant (NPP) structures. Therefore, the safety against EQ of structural and non-structural components (NSCs) in NPP is a critical concern. In particular, the safety concern of the NPP structures has significantly increased since the Fukushima Daiichi nuclear accident in Japan (2011) and the Gyeongju (2016) and Pohang (2017) EQs in South Korea [1, 2]. The auxiliary building (AB) is one of the main parts of NPP systems. AB is generally placed adjacent to the reactor containment structure that supports most of the auxiliary and safety-related systems and components [3]. The configuration for the structural and NSCs in NPP has been reported by Kwag et al. [4] as shown in Figure 1. NSCs are susceptible to earthquakes throughout the last few decades [5]. Some damages of NSCs due to EQ events are depicted in Figure 2, captured by Jiang [5]. The AB contains many substantial NSCs, i.e., pumps, heat exchanger, feedwater tanks, main control room, emergency diesel generator, fuel storage tanks, radioactive waste systems, chemical and volume control systems, etc. [3, 6]. In the context of safety assurance and operating the NPP, the seismic analysis, design, assessment, and evaluation of such NSCs are the most challenging issue. Besides, the distribution of the following NSCs plays a vital role in minimizing the seismic responses without addition and any structural modification.

*Corresponding Author Institutional Email: kim2kie@kongju.ac.kr (D. Kim)

Please cite this article as: M. M. Rahman, T. T. Nahar, D. Kim, D. W. Park, Location Sensitivity of Non-structural Component for Channel-type Auxiliary Building Considering Primary-secondary Structure Interaction, ***International Journal of Engineering, Transactions A: Basics***, Vol. 35, No. 07, (2022) 1268-1282

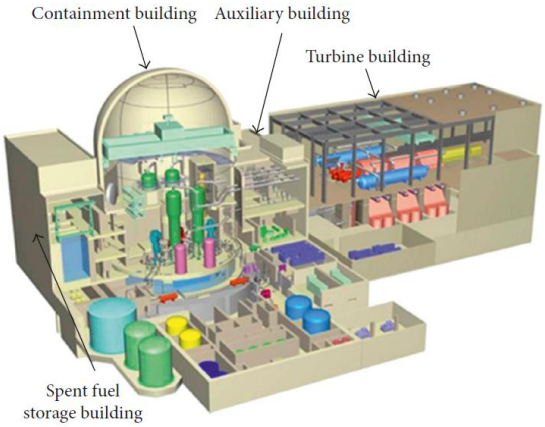

Figure 1. NPP with structural and NSCs systems [4]

Figure 2. Earthquake damage of NSCs [5]

The previous study focuses mainly on the vertical distribution of NSCs. Hur et al. [7] investigated the seismic performance of nonstructural components located in various locations throughout the AB and found that the probability of acceleration of NSCs on the first floor is greater than that of NSCs on the second floor. Mondal and Jain [8] recommend, for the design of NSCs and their attachments, amplification of lateral force that increases with an increase in vertical position of the NSCs should be considered. If the NSC is located on lower building floors and has a natural period equal to or greater than the building's second or third natural period, the responses of NSCs are amplified [9]. Merz and Ibanez [10] reported only for rough estimates of NSCs, floor response spectra (FRS) may be considered but estimating the mounting point response is desirable. According to Pardalopoulos and Pantazopoulou [11], the responses of NSCs are mainly controlled by the developed absolute spectral acceleration at the mounting point on the supporting building. However, there are no considerable investigations on the previous study for the response behavior of NSCs attached at different locations on the same floor.

This type of distribution can be very effective in response measures of NSCs; especially for the asymmetric building which is the main motivation of this study. This study evaluates the location sensitivity on NSCs on the same floor under earthquake excitation considering the primary-secondary structure interaction. To fulfill the objective of this study, the numerical investigations were conducted using a three-dimensional finite element model (FEM) developed by SAP2000 software [12] of a channel type AB. This building was designed and the shake table test program was organized by the Korea Atomic Energy Research Institute (KAERI). Among various modal parameter estimation (MPE) techniques, least-squares complex exponential (LSCE) was utilized for MPE using the shake table test results. LSCE approximates the correlation function using the sum of exponentially decaying harmonic functions [13-16]. After evaluating the modal parameters, the FEM was updated based on test results through a statistical tool, i.e., response surface methodology (RSM). Many researchers employed the RSM for FEM optimization due to its simplicity and effectiveness [17-23]. Then the evaluation was conducted using optimized FEM throughout the study.

2. AUXILIARY BUILDING

As demonstrated in Figure 3(a), this study was conducted using a channel type three-storied AB provided by KAERI. The overall dimension of the main part of the test specimen is 3650mm×2575mm×4570mm. The thicknesses of slabs, walls, and base assembly are 140mm, 150mm, and 400mm, respectively. The detailed dimensions of the test specimen are predicted in Figure 3(b).

2. 1. Shake Table Test The Earthquake Disaster Prevention Center at Pusan National University conducted this experimental program with the shaking table facility. This program was organized by KAERI for joint research on the Round Robin Analysis to evaluate the dynamic characteristics and to verify the numerical model for the AB in NPP. To capture linear response characteristics, natural frequencies, and vibration modes, the model was initially excited by a low-intensity random vibration (peak acceleration is 0.05g) in X and Y-directions separately [24].

The sensors, i.e., the accelerometers were installed as different arrays to record the responses under the excitation in X and Y direction. Figure 4(a) and Figure 4(b) show the accelerometer's location for X and Y-directional responses, respectively. Although the shake

table test was directed for the Gyeongju earthquake with a loading sequence as 0.28g - 0.28g - 0.50g - 0.75g - 1.00 g, which was not considered in this study. The random vibration response was utilized for MPE and validates the linear FEM model of the AB.

(a)

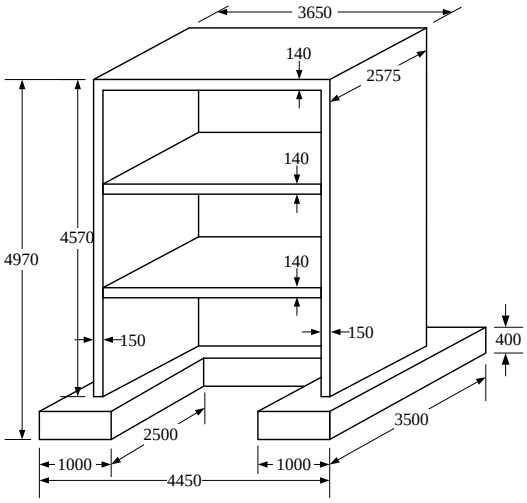

(b)

Figure 1. Test specimen (a) Anchorage system, (b) Dimension details

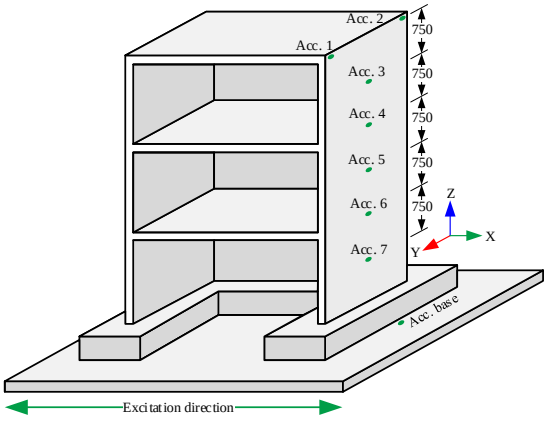

(a)

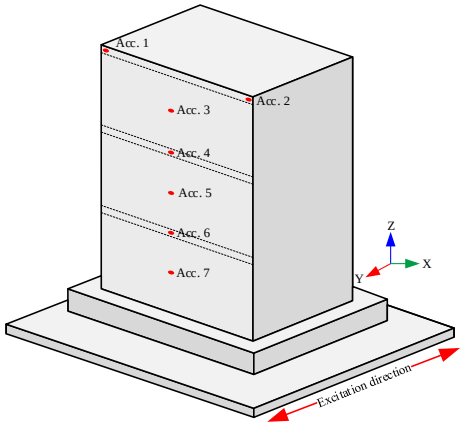

(b)

Figure 4. Sensor's location for record the responses (a) X-direction and (b) Y-direction

Figure 5(a) and Figure 5(b) represent the recorded acceleration response for the X and Y-direction, respectively. Here, the sensors denoted as "Acc. base", "Acc. 6", "Acc. 4" and "Acc. 1" are the sensors for the corresponding base, 1st floor, 2nd floor, and 3rd floor (roof) responses for each case, which is used for MPE.

In the study, the LSCE method was used for MPE. Figure 5(a) and Figure 5(b) illustrate the stabilization diagram for X and Y-direction the input-output responses of shake table test for probable model order and a frequency range up to 30 and 100Hz, respectively. The dot marker specifies the unstable poses whereas plus-shaped shows stable one in frequency and damping, and the circular marker represents the stale poles only in frequency. Furthermore, a solid blue line depicts the average response to help distinguish between physical and non-physical poles. The modal frequency of predominant modes, i.e., mode 1 (X-direction) and mode 2 (Y-direction) are 16.05 Hz and 23.02 Hz (Figure 6). The damping ratio for fundamental modes varies from

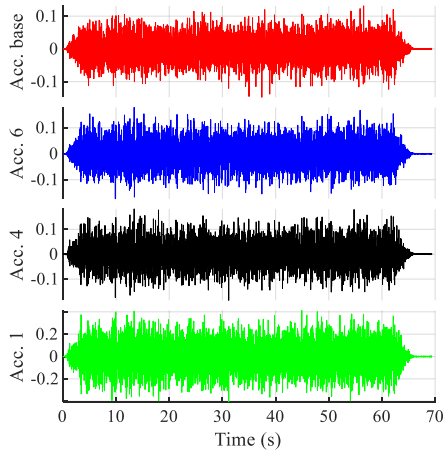

(a)

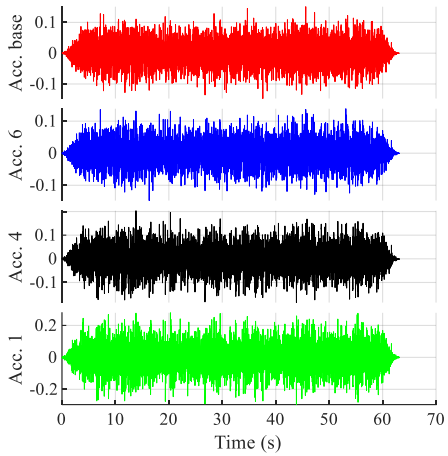

(b)

Figure 5. Stabilization diagram from shake table test results (a) X-direction and (b) Y-direction

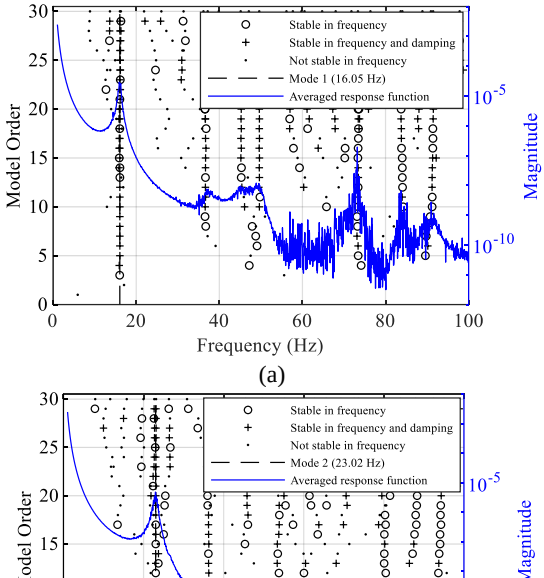

(a)

(b)

Figure 6. Stabilization diagram from shake table test results (a) X-direction and (b) Y-direction

3.18 to 3.74% according to the LSCE. Details about MPE using LSCE has been reported by Rahman et al. [24].

2. 2. Numerical Modeling and Updating For the dynamic evaluation of horizontally distributed NSCs, i.e., secondary structures on the KAERI channel type AB, a three-dimensional linear (elastic) FEM developed using commercially available structural analysis and design software SAP2000 is presented in this study [12]. SAP2000 allows the nonlinear behavior of materials to be modeled using either link/support elements or plastic hinges or multilayer shell elements [12, 25]. During the shake table test evaluation, the building was excited under the Gyeongju earthquake (2016) with a loading sequence as 0.28g - 0.50g - 0.75g - 1.00 g. When the excitation level was upto 1.00 g, there was no remarkable damage present in the structure [2]. Also, the maximum floor acceleration i.e., zero period acceleration (ZPA) responses in the incremental dynamic analysis (IDA) as shown in Figure 7, indicates that the building model shows approximately linear behavior up to 1g excitation level of peak table acceleration (PTA). Therefore, in this case, linear analysis was performed.

The slabs and walls were modeled as 4 noded shell elements. And the base assembly was considered as 8 noded solid elements. The maximum mesh size is assumed as 300mm. Figure 8(a) shows the full FEM with mesh view. As the shear wall elements were assumed as elastic, the effective stiffness was considered to reduce the strength for inelastic behaviors. Based on ACI [26], the effective stiffness was applied by reducing the moment of inertia (I_g) of the wall as $0.70I_g$ (as it was in uncracked condition). The NSCs were modeled by the linear spring available in SAP2000 which were rigidly connected with the mounting position as depicted in Figure 8(b). Three translational degrees of freedoms (Ux, Uy, and Uz) were activated at the top of NSCs. The second floor was considered for the placing of NSCs in this case study. The governing equation of motion for linearly modeled structure can be expressed as Equation (1) [27]:

$$M\ddot{u}(t) + C\dot{u}(t) + Ku(t) = -M\ddot{u}_g(t) \quad (1)$$

where $\ddot{u}$, $\dot{u}$, and u represent the acceleration, velocity, and displacement vector of the systems at any instant of time (t). $\ddot{u}_g$ denotes the ground motion excitation acceleration. The compiled mass (M), damping (C) and

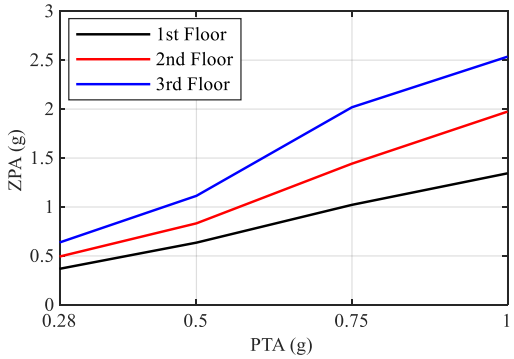

Figure 7. Shake table test, IDA Responses of building under Gyeongju earthquake (2016)

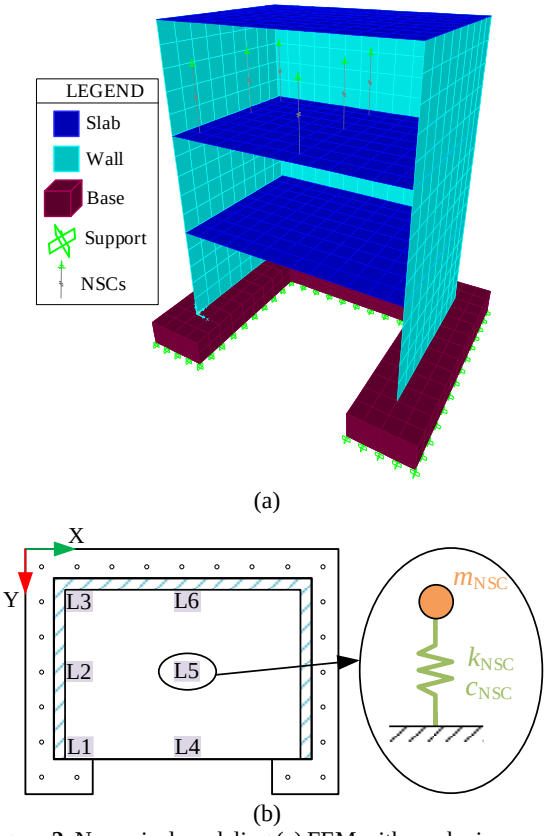

Figure 2. Numerical modeling (a) FEM with mesh view, and (b) probable location and SDF system of NSC

stiffness (K) matrices considering primary-secondary structure interaction can be expressed by Equation (2) [28]:

$$M = \begin{bmatrix} m_{\mathrm{p}} & 0 \\ 0 & m_{\mathrm{NSC}} \end{bmatrix};$$
$$C = \begin{bmatrix} c_{\mathrm{p}} & 0 \\ 0 & c_{\mathrm{NSC}} \end{bmatrix}; \quad (2)$$
$$K = \begin{bmatrix} k_{\mathrm{p}} & 0 \\ 0 & k_{\mathrm{NSC}} \end{bmatrix}$$

where the mass matrix for primary and secondary structures are denoted by m_{p} and m_{NSC}, respectively. c_{p} and c_{NSC} denote the damping matrix of primary and secondary structures and finally, the stiffness matrix of primary and secondary structures are symbolized by k_{p} and k_{NSC}, respectively.

For the case study, the height and masses of NSCs are implicit as 1m and 200kg. The global damping matrix (C) of the coupled system was constructed by assuming the same damping ratio (3.4%) for primary and secondary structures. The stiffness of the NSCs was calculated as, $k_{\mathrm{NSC}} = 4\pi^2 f_{\mathrm{NSC}}^2 m_{\mathrm{NSC}}$. The frequency range of NSCs was assumed as 5 to 50Hz. The evaluation was directed by a frequency increment of 5Hz.

Before going to the evaluation stage, the FEM was calibrated using RSM based on the updating of concrete material properties. The RSM is a collection of statistical models that may be used to model, analyze, optimize, and construct an empirical model [29]. It appears to be highly promising in terms of reducing the time and cost of model design and analysis [30].

Based on the statistical and mathematical analysis, RSM investigates the approximate relationship of the input design variables and the outputs in the form of a linear or polynomial equation. According to Rastbood et al. [19], a polynomial of higher-order must be used, if the system has curvatures and in most cases, the second-order is adequate to handle engineering problems [21]. Therefore, a second-order polynomial equation is considered for the RSM as shown in Equation (3) to get the response, y.

$$y = \beta_0 + \sum_{i=1}^{k} \beta_i x_i + \sum_{i=1}^{k} \beta_{ii} x_i^2 + \sum_{i=1}^{k} \sum_{i<j}^{k} \beta_{ij} x_i x_j + \varepsilon \quad (1)$$

where the intercept, linear, quadratic, and interaction terms are represented by β_0, β_i, β_{ii}, and β_{ij}, respectively; k denotes the number of input variables and ε is the offset or residual related to the experiments.

The central composite design (CCD) was used to estimate the number of the experiment of RSM for optimization of multi-objective input variables [31]. The total number of samples of runs of the experiment required for a complete CCD circumscribed is computed by $N = 2^k + 2k + n_c$; where k is the number of factors, i.e., input variables; and 2^k, $2k$, and n_c represent the number of cubic, axial, and center points. Here, each factor is studied at 5 levels as depicted in Figure whereas one center point, two cubic points, and two axial points are established at a distance -α and +α which represent new extreme values. The α value of 1.682 was calculated considering the full factorial CCD by $\alpha = [2^k]^{1/4}$ [32].

A total of 3 factors were used, i.e., Young's modulus (E), mass density (ρ), and Poisson's ratio (μ) as input variables, and 2 parameters are considered as responses, i.e., modal frequency of mode 1 ($F1$) and mode 2 ($F2$).

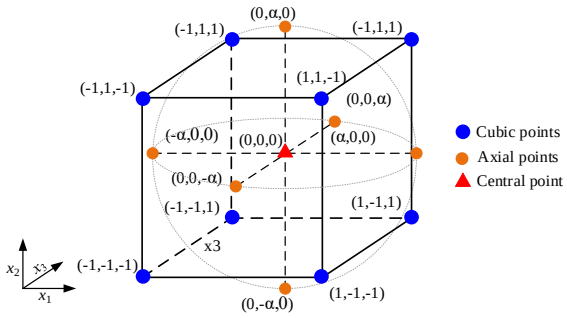

Figure 9. Central Composite Design (CCD) coded points

The lower and upper limit ranges of factors were chosen based on the normal concrete material properties. The range for density and Poisson's ratio was 0.15 to 0.25 [33] and 2200 to 2600 kg/m^3 [34], respectively. The Young's modulus was assumed to be 10 to 25 GPa. The cubic, axial and central points coded and actual values of 3 factors are presented in Table 1.

CCD created a total of 20 design points for E, ρ, and μ. Each set of design points and corresponding responses from FEM are listed in Table 2.

TABLE 1. Factors value range from CCD

Factors	Range	Cubic		Axial		Central
		Min.	Max.	Min.	Max.	
E	CVR	-1	+1	- α	+ α	0
	AVR	10	25	4.89	30.11	17.5
ρ	CVR	-1	+1	- α	+ α	0
	AVR	2200	2600	2063.64	2736.36	2400
μ	CVR	-1	+1	- α	+ α	0
	AVR	0.15	0.25	0.12	0.28	0.20

CVR: Coded value range; AVR: Actual value range; unit for actual values of E and ρ are GPa and kg/m3, respectively.

TABLE 2. Input factors and responses

Run order	Inputs/ Factors			Outputs			
	1	2	3	FEM		RSM	
	E (GPa)	ρ (kg/m3)	μ	F1 (Hz)	F2 (Hz)	F1 (Hz)	F2 (Hz)
1	4.89	2400	0.2	8.74	12.96	8.98	13.32
2	17.5	2400	0.17	16.64	24.71	16.67	24.76
3	10	2200	0.25	13.01	19.30	12.91	19.15
4	10	2600	0.25	11.97	17.75	11.85	17.58
5	17.5	2400	0.2	16.53	24.53	16.53	24.53
6	25	2600	0.25	18.93	28.07	18.98	28.15
7	17.5	2400	0.2	16.53	24.53	16.53	24.53
8	25	2200	0.15	20.71	30.75	20.78	30.86
9	25	2200	0.25	20.57	30.52	20.64	30.62
10	10	2200	0.15	13.10	19.45	13.00	19.30
11	17.5	2400	0.2	16.53	24.53	16.53	24.53
12	17.5	2400	0.2	16.53	24.53	16.53	24.53
13	30.11	2400	0.2	21.69	32.18	21.51	31.93
14	17.5	2400	0.2	16.53	24.53	16.53	24.53
15	17.5	2736.36	0.2	15.48	22.98	15.54	23.06
16	10	2600	0.15	12.05	17.89	11.93	17.71
17	17.5	2400	0.28	16.45	24.39	16.49	24.45
18	25	2600	0.15	19.05	28.29	19.11	28.37
19	17.5	2400	0.2	16.53	24.53	16.53	24.53
20	17.5	2063.64	0.2	17.83	26.46	17.84	26.48

The polynomial relationships between input variables (for E, ρ, and μ) and responses ($F1$ and $F2$) from Equation (3) can be presented by Equations (4). The coefficients for Equations (4) using RSM through the Minitab tool [35] are shown in Table 3.

$$F1 \text{ or } F2 = \beta_0 + \beta_1 E + \beta_2 \rho + \beta_3 \mu + \beta_{11} E^2 + \beta_{22} \rho^2 + \beta_{33} \mu^2 + \beta_{12} E\rho + \beta_{13} E\mu + \beta_{23} \rho\mu \quad (4)$$

The analysis of variance (ANOVA) established by Ronald Fisher in 1918, is an effective method for assessing the model fitness [36, 37]. To clarify the model fitness with data, the probability values (P-value) are compared to their significant level. Model terms with P-values less than 0.05 are considered significant. Model terms are significant if the P-value is less than 0.05. Table 4 indicates that for both responses ($F1$ and $F2$), E, ρ, E^2, and $E * \rho$ are significant model terms. The model F-value of 1409.60 and 1409.09 for $F1$ and $F2$, respectively implies the model is significant. The goodness of fit, i.e., R^2 is 99.92% and also the Predicted R^2 of 99.40% is in reasonable agreement with the Adjusted R^2 of 99.85% for both models (Table 5). Therefore, the model represented in Equation (4) for $F1$ and $F2$ prediction can be used.

To make it easier to grasp, the surface plot function was used to display a three-dimensional perspective of the response when the parameters were changed. Figures 10 and 11 show the response plot (surface and contour) using Equation (4) for corresponding output variables $F1$ and $F2$, respectively. It shows that the changing pattern of responses $F1$ and $F2$ with respect to factors E and ρ is approximately similar.

To get the optimized value of E, ρ, and μ the target values for $F1$ and $F2$ were set to 16.05 and 23.02 Hz. The optimized values for E, ρ, and μ were 15.75 GPa, 2400 kg/m^3, and 0.20, respectively (Figure 13). Figure 13 demonstrates that the values of $F1$ and $F2$ are matched

TABLE 3. Value for coefficients in Equations

Coefficients	Responses	
	$F1$	$F2$
β_0	18.03	26.69
β_1	1.0293	1.529
β_2	-0.00852	-0.01259
β_3	-4.1	-6.1
β_{11}	-0.008071	-0.011979
β_{22}	0.00000142	0.0000021
β_{33}	7.5	10.6
β_{12}	-0.000101	-0.00015
β_{13}	-0.033	-0.056
β_{23}	0.00025	0.00039

TABLE 2. ANOVA of RSM model

Responses	Source	DF	Adj SS	Adj MS	F-Value	P-Value
	Model	9	199.595	22.177	1406.60	0.000
	E	1	189.806	189.806	12038.58	0.000
	ρ	1	6.395	6.395	405.62	0.000
	μ	1	0.042	0.042	2.64	0.135
	E^2	1	2.970	2.970	188.40	0.000
	ρ^2	1	0.047	0.047	2.96	0.116
	μ^2	1	0.005	0.005	0.32	0.584
$F1$	$E * \rho$	1	0.185	0.185	11.72	0.007
	$E * \mu$	1	0.001	0.001	0.08	0.788
	$\rho * \mu$	1	0.000	0.000	0.00	0.956
	Error	10	0.158	0.016		
	Lack-of-Fit	5	0.158	0.032		
	Pure Error	5	0.000	0.000		
	Total	19	199.752			
	Model	9	439.571	48.841	1409.09	0.000
	E	1	417.989	417.989	12059.13	0.000
	ρ	1	14.085	14.085	406.36	0.000
	μ	1	0.120	0.120	3.46	0.093
	E^2	1	6.543	6.543	188.76	0.000
	ρ^2	1	0.101	0.101	2.92	0.118
	μ^2	1	0.010	0.010	0.29	0.602
$F2$	$E * \rho$	1	0.407	0.407	11.75	0.006
	$E * \mu$	1	0.003	0.003	0.10	0.758
	$\rho * \mu$	1	0.000	0.000	0.00	0.954
	Error	10	0.347	0.035		
	Lack-of-Fit	5	0.347	0.069		
	Pure Error	5	0.000	0.000		
	Total	19	439.918			

TABLE 5. RSM model summary

Responses	S	R^2 (%)	Adjusted R^2 (%)	Predicted R^2 (%)
$F1$	0.126	99.92	99.85	99.40
$F2$	0.186	99.92	99.85	99.40

S: standard deviation

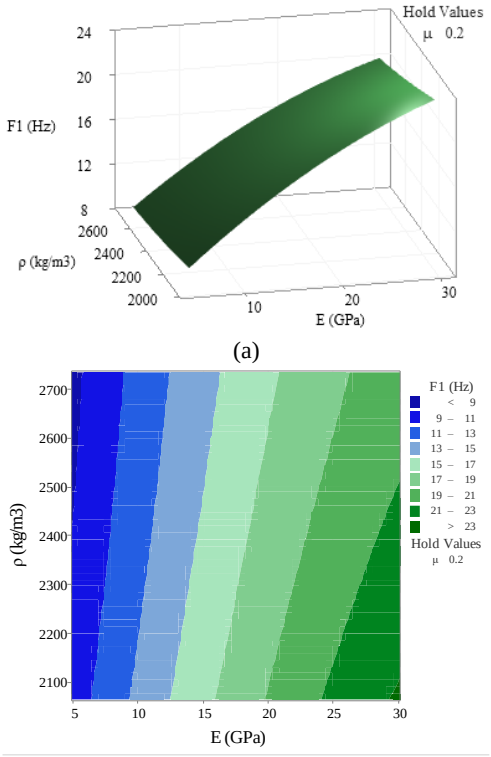

Figure 10. Response plot for $F1$ Vs E and ρ (a) surface plot and (b) contour plot

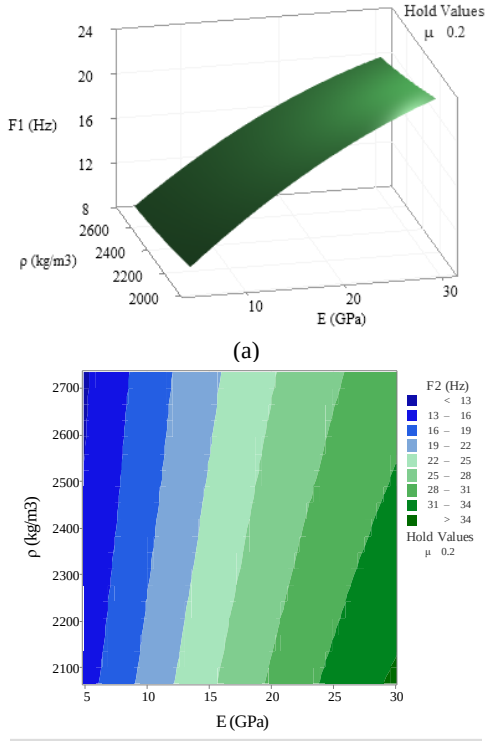

Figure 11. Response plot for $F2$ Vs E and ρ (a) surface plot and (b) contour plot

about 94 and 98%, respectively with the target values and the composite desirability is matched about 96%. Figure 12(a) depicted the comparison of actual responses of $F1$ and $F2$ were from FEM and the predicted responses using RSM (Equation (4)). The results from both models are near to the diagonal (dotted line), showing a good correlation between the predicted and actual values. Figure 12(b) shows that the maximum error between the fitted values from RSM and the FEM simulation is 2.75%, which also relay the use of the predicted model for further study.

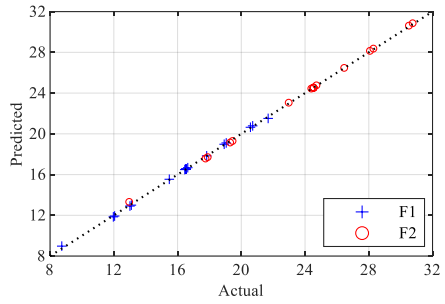

Figure 12. (a) Predicted vs. Actual plot, (b) Error of fitted values from RSM

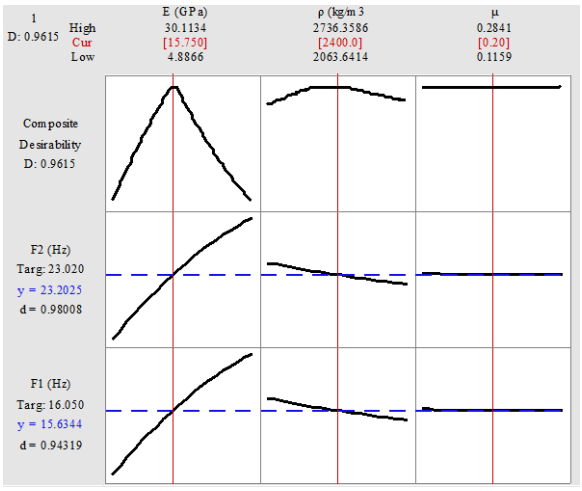

Figure 13. Modal frequency optimization plot (using Minitab tool)

2. 3. Model Validation The FEM model was validated through the modal parameters and the response function under random seismic excitations. The MPE is the first stage in detecting structural deterioration and performing structural health monitoring (SHM) or assessing dynamic characteristics. The natural frequencies of the AB were obtained through modal analysis, and the results were compared with shake table test results to validate the studied FEM. The most fundamental frequencies (mode 1 and mode 2) are enlisted in Table 6 along with the error compared with test results. The mode shapes (first 6 modes) and their natural frequencies along with modal participation mass ratio (MPMR) from FEM are described in Figure .

Table 6 shows that the maximum error is 2.4%, which indicates the good agreement of the result from FEM in this study with compared to shake table test. Based on the LSCE methods, the magnitudes of the averaged response functions were plotted against frequencies as shown in Figure 15, which also indicate similar dynamic actions between the actual model and FEM. Therefore, the presented model was used for the NSC's location sensitivity evaluation.

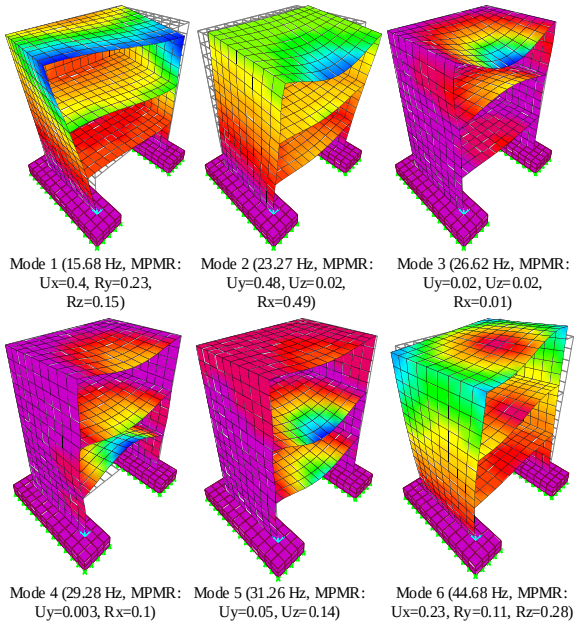

Figure 14. Fundamental mode shapes

TABLE 3. Fundamental frequencies of APR1400 NPP model

Modes	Modal frequency, F (Hz)		
	Shake table test	FEM	Error $\left(\frac{\lvert F_{test}-F_{FEM}\rvert}{F_{test}}\right)$
Mode 1	16.05	15.68	2.4%
Mode 2	23.02	23.27	1.1%

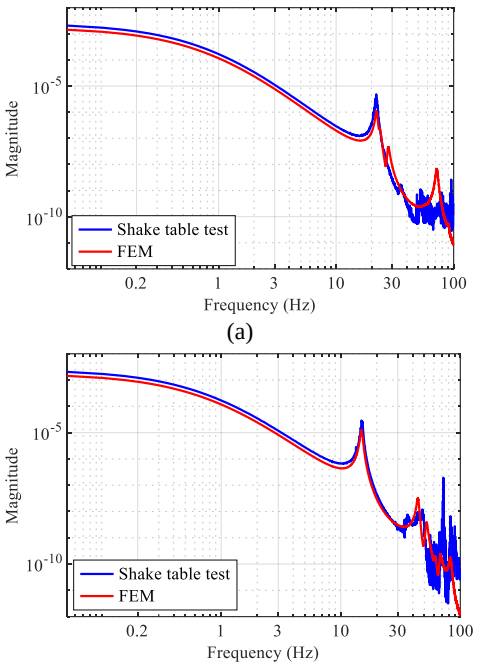

Figure 15. Average response function from shake table and FEM results (a) X-direction and (b) Y-direction

3. LOCATION SENSITIVITY ANALYSIS

3. 1. Input Ground Motions (GMs) To evaluate the response behavior of NSCs, two types of input motions were used, i.e., 1) artificially generated GMs (AGMs) for the reference design response spectrum (DRS), and 2) Sine sweep with exiting frequency range 5 to 50 Hz. The artificial ground motion was generated for the response spectrum compatible accelerogram for the design of NPP, i.e., Regulatory guide 1.60 (RG 1.60) [38]. The GMs were applied in three directions, i.e., horizontal 1, H1 (X-direction); horizontal 2, H2 (Y-direction); vertical, V (Z-direction). The peak acceleration for the horizontal component was considered based on 2400 years of return period for seismic zone I (Korean peninsula), i.e., 0.22g [39]. The vertical component of GM was defined by scaling of the horizontal component by a factor of 2/3, i.,e., 0.147 [40]. The generation was done using the Matlab-based computer tool "Quake_M" developed by Kim and Quake [41] as represented in Figure 16 and Figure 17(a). The root means square error of AGMs are 1.004%, 1.187%, and 0.729% for H1, H2, and V directions, which indicate the well-matched AGMs with target spectrum (RG 1.60). The sine sweep was used to confirm the response behavior for all excitation modes (target frequency range) of the NSCs. The amplitude of the sine sweep was the same as AGMs. Only the first 3s of sine sweep is presented in Figure 17(b) for the clear visualization, but actually it was 30s with frequency range 5 to 50 Hz.

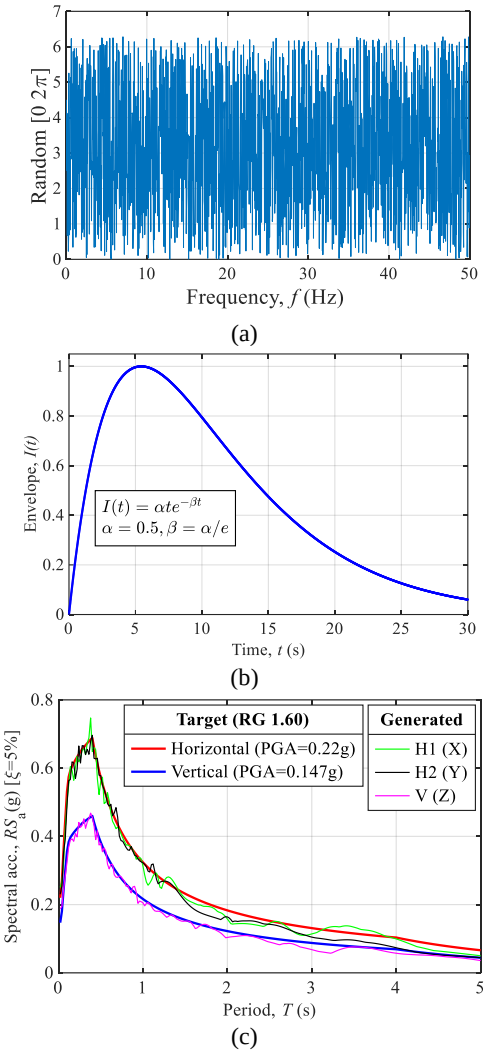

Figure 16. Generation of spectra-matched AGMs (a) Seed function: white noise, (b) Envelope function and (c) Target and generated response spectrum

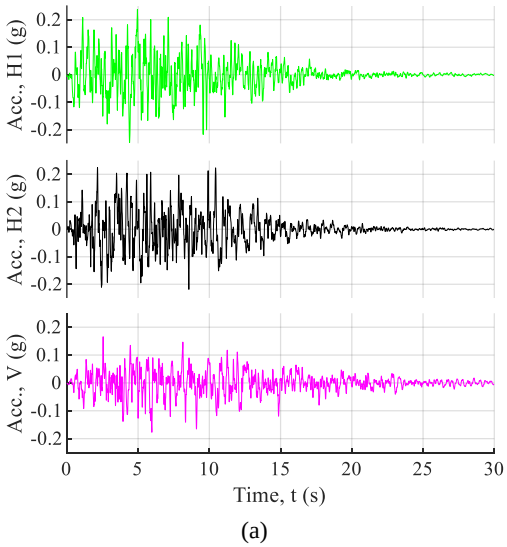

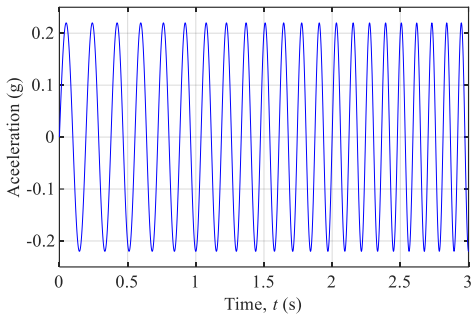

(b)

Figure 17. Input GMs (a) Generated AGMs (target: RG 1.60 DRS) and (b) Sine sweep (0~3s)

3. 2. Location Sensitivity To evaluate the location sensitivity of NSCs, a total of 6 probable locations as shown in Figure 8(b) were considered in this study, i.e., 1) L1 represents the response of outside or exposer corners, 2) L2 denotes the middle of the sidewall, 3) L3 indicates the responses for the inside corners, 4) L4, middle of the exposer side of the building, 5) L5, middle of the floor, 6) L6, which replicates the responses of the middle of the back wall of the AB. The study was conducted assuming the NSCs are distributed only on the second floor.

Zero period acceleration (ZPA) i.e., peak acceleration responses are compared for each direction and each loading. Figure 18 replicates the acceleration responses in X-direction whereas Figure 19 shows the corresponding ZPA of NSCs placed in each credible location, in which the responses for L1 and L4, L2 and L5, and L3 and L6 indicate the similar path under AGM and sine sweep as well. In the case of AGM excitation,

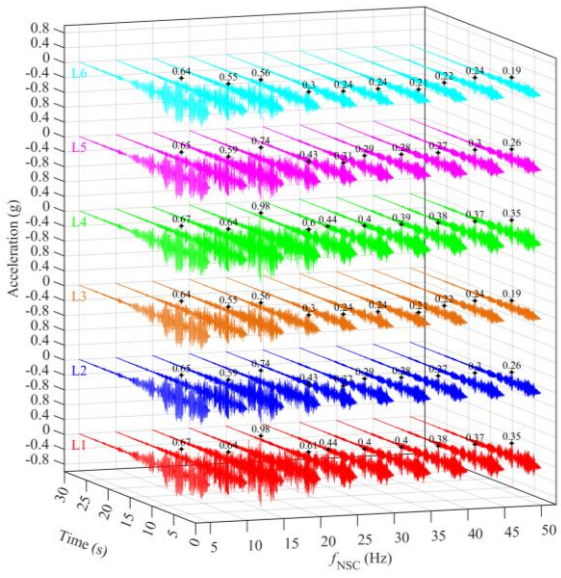

(a)

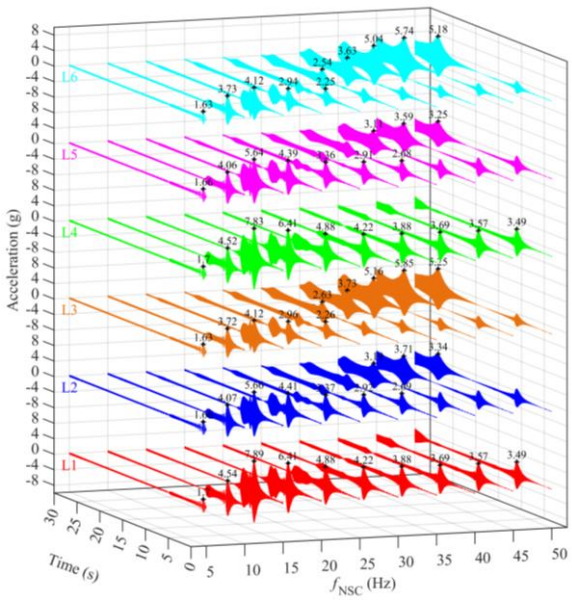

(b)

Figure 18. Acceleration responses in X-direction (a) AGM excitation (b) Sine sweep excitation

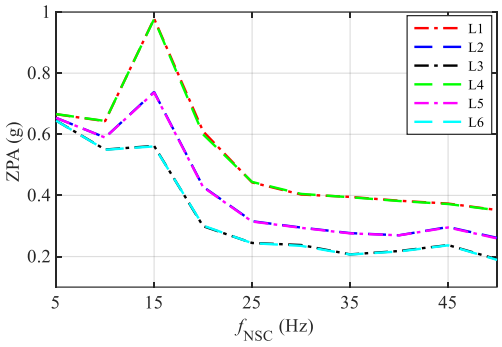

(a)

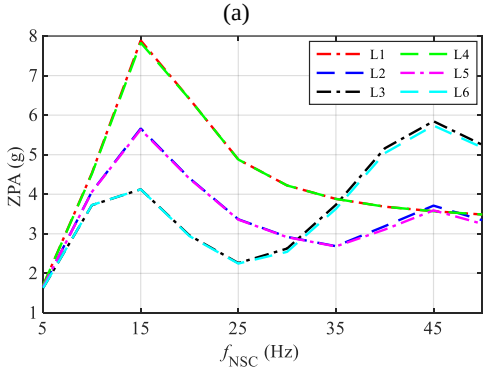

(b)

Figure 19. X-directional ZPA responses of NSC (a) AGM excitation (b) Sine sweep excitation

the NSCs with frequency around 15Hz were more vulnerable (in X-direction) under both excitation for location L1 and L4. Additionally, it confirms that the NSCs with higher frequency, i.e., around 45Hz were

more sensitive for location L3 and L6 than others under sine sweep excitation.

In Y-directional response as shown in Figure 20, the AGM excitation indicates that if NSCs frequency is more than the 1st modal frequency of AB, the locations for L1, L2 and L3 are more sensitive than others, whereas the sine sweep excitation reveals that all locations were pursuing approximately the similar track and sensible frequency range was widespread (it may be 15Hz to 35Hz) (Figure 21). Figure 22 explores the time history responses for all considered locations in Z-direction. Figure 23 ensure that in Z-direction the riskier zone was in the middle of the exposure side, i.e., L4, and also the NSCs with frequency around 25Hz in this zone were more hazardous than others.

There are different types of NSCs in NPP, electrical cabinet is one of them, which plays a critical role in the

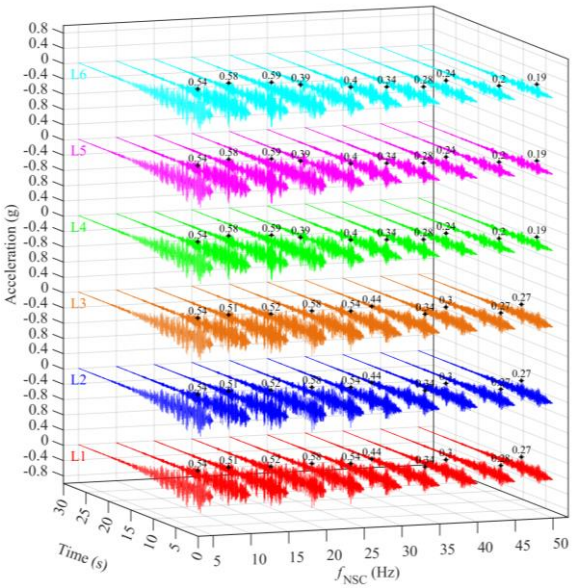

(a)

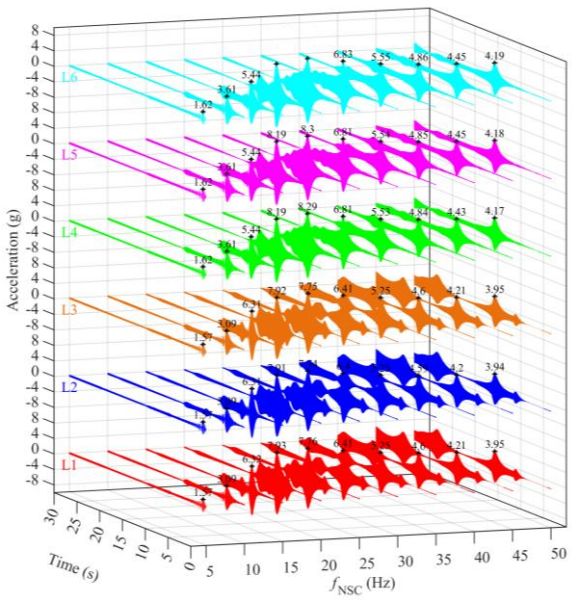

(b)

Figure 20. Acceleration responses in Y-direction (a) AGM excitation (b) Sine sweep excitation

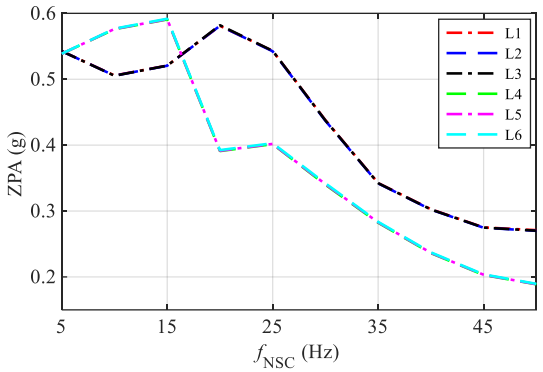

(a)

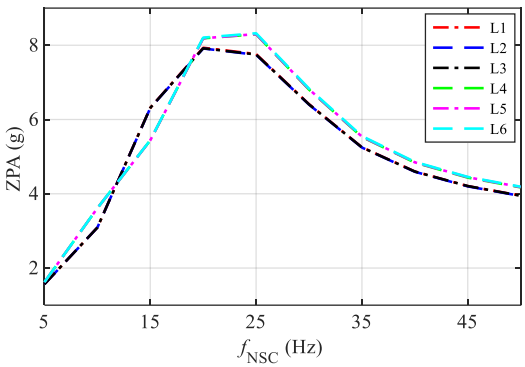

(b)

Figure 21. Y-directional ZPA responses of NSC (a) AGM (b) Sine sweep excitation

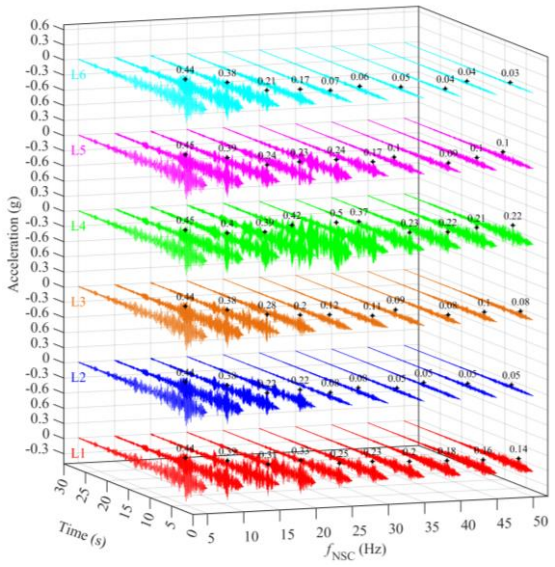

(a)

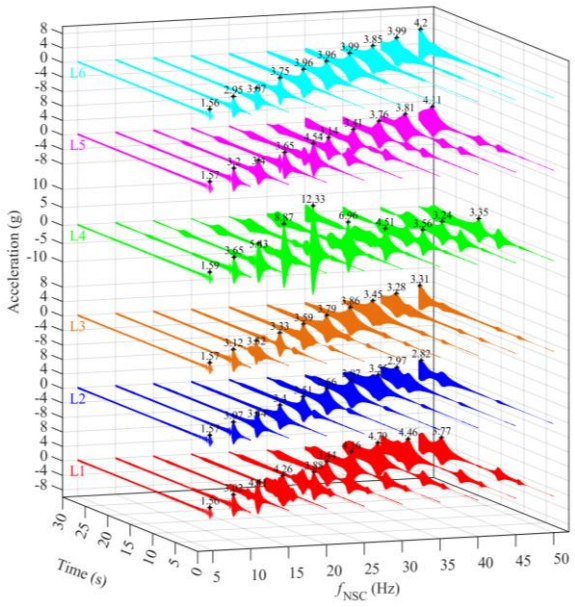

(b)

Figure 22. Acceleration responses in Z-direction (a) AGM excitation (b) Sine sweep excitation

proper functionality of NPP [42]. Like other NSCs, the cabinet is also acceleration sensitive so it can be susceptible to the high-frequency input motions. Here, as a case study, a single electrical cabinet was used to check the location sensitivity on the response under AGMs. The properties, i.e., stiffness (2897kN/m) and mass (287kg) of the cabinet were obtained from Salman et al. [28]. The cabinet was modeled for both directions, i.e., X and Y-directions using same the mass and stiffness values (Z direction was considered as fully stiff). Figure 24(a) shows the cabinet response spectrum under AGMs and it reflects that the location L1 and L4 give 61.8% more peak spectrum acceleration than L3 and L6 for X-direction. Similarly, in Y-directional responses, the L4, L5, and L6 were more sensible (21.5%) than other locations (Figure 24(b)). So, the cabinet or other NSCs distribution over the same floor is very important to get the proper in-cabinet response spectrum for selecting the engineering demand parameters (EDP). From Figure 25, it can be concluded that considering the ZPA as EDP, the L3 location is the best choice for electrical cabinet, which can provide safety of devices in the cabinet by lowering (around 42% in X and 15% in Y-direction) the ZPA responses.

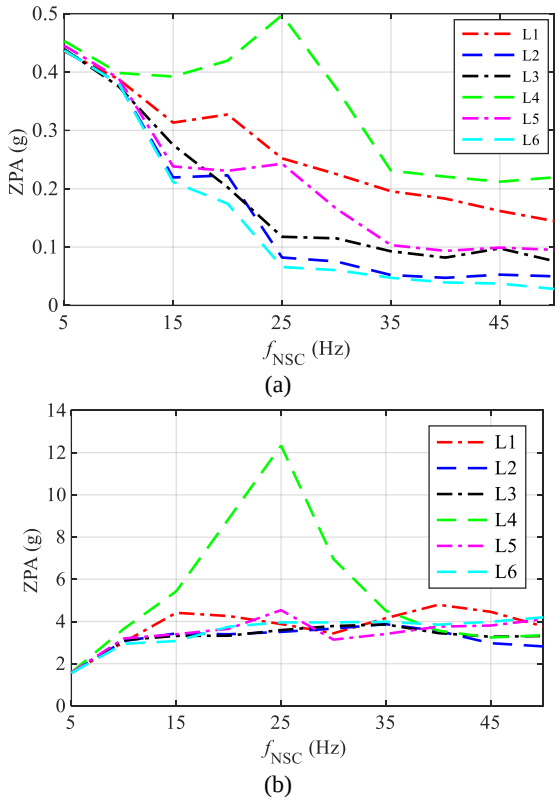

(a)

(b)

Figure 23. Z-directional ZPA responses of NSC (a) AGM excitation (b) Sine sweep excitation

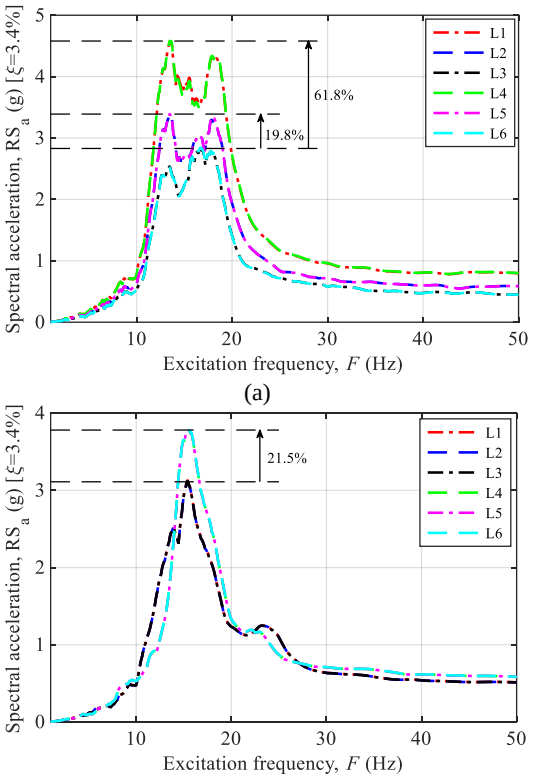

(a)

(b)

Figure 24. Response spectra of electrical cabinet under AGM (a) X-direction, (b) Y-direction

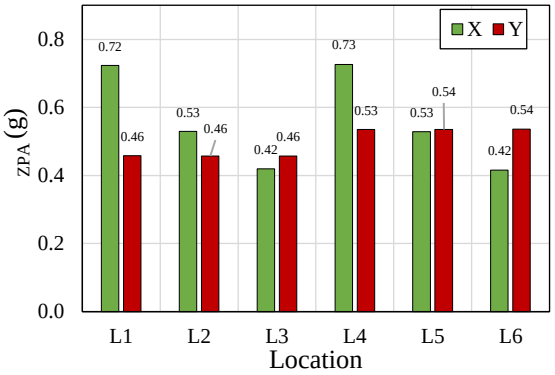

Figure 25. ZPA responses of the cabinet under AGM

4. CONCLUSIONS

The effects of the distribution of NSCs over the same floor in an AB under seismic excitations have been focused. Most of NSCs in NPP are acceleration sensitive and the floor acceleration can differ in the different mounting positions of NSCs. The flexibility of floor and combination of predominant modes with translational and torsional effects (especially in channel-type buildings) can lead to diverse responses of them in different locations. Therefore, the location sensitivity needs to be assessed before placing the NSCs in NPP to reduce the responses. KAERI channel type AB was acted here as the reference for developing the FEM to capture the goal through numerical evaluation. The FEM was calibrated using RSM and the calibrated model was used for seismic analysis under AGMs and sine sweep excitation for NSCs with frequency range 5 to 50Hz, which was rigidly mounted on six different locations. Finally, the sensitivity of the response of NSCs was evaluated for different locations. The key findings and conclusions from the results can be summarized as follows:

• In X-direction, the exposer side corners (L1) and mid positions (L4) are more vulnerable especially if the frequency of NSCs (around 15 Hz) are around the first mode of AB. Although, the inside corners (L3) and middle of the back wall (L4) show lower responses for AGMs whereas sine sweep confirms that after 30 Hz (frequency of NSCs) L3 and L4 increase the responses remarkably (especially around 45 Hz).

• In Y-direction, if the NSCs frequency is less than 15Hz the exposure corners (L1), middle of the sidewall (L2), and inside corners (L3) are more sensitive. If the frequency is more than 20Hz the response behavior changes and in this case, the middle of the exposure side (L4), middle of the floor (L5), and middle of the back wall (L6) show more sensitivity. However, under sine sweep, the sine sweep excitation reveals that all locations are pursuing approximately a similar track and sensible frequency range is widespread (around 2nd and 3rd modes of the AB).

• In Z-direction, the riskier zone in the middle of the exposure side (L4), and also the NSCs with frequency around 25Hz in this zone is more hazardous than others.

• The location selection of NSCs can be reduced up to 30% horizontal (X or Y-direction) and 70% vertical ZPA responses which can lead to the economic design of NSCs as there is no need to consider any additional measures, just the right choice of mounting positions based on their vibration frequency.

• In the case of the cabinet, the inside corners (L3) can be a good choice for the placement and the middle of the exposure side (L4) will be the worst choice. Placing at L3 can reduce the maximum cabinet response spectrum by around 62% in X-direction and 22% in Y-direction, which were measured under AGMs excitation.

4. FUNDING

This work was supported by the National Research Foundation of Korea (NRF) grant funded by the Korea government (MSIT), Grant No.: 2021R1A4A1031509.

5. REFERENCES

1. Kim, N. and Kim, M., "Investigation of existing researches for seismic fragility assessment of fuel assembly in NPPs", in Transactions of the Korean Nuclear Society Virtual spring Meeting, Online, Korean Nuclear Society, (2021), 2021.
2. Kim, M., Jung, J.-W., Ha, J.-G., Hahm, D. and Moon, H.S., *The Shaking Table Test of Shear Wall Structure for Seismic Performance Evaluation of Nuclear Power Plants*. 2021, Korea Atomic Energy Research Institute: Daejeon, Korea.182.
3. NRC, U.S. *Auxiliary building*. 2021 March 09, 2021 [cited 2021 July 01]; Available from: https://www.nrc.gov/reading-rm/basic-ref/glossary/auxiliary-building.html.
4. Kwag, S., Ju, B. and Jung, W., "Beneficial and Detrimental Effects of Soil-Structure Interaction on Probabilistic Seismic Hazard and Risk of Nuclear Power Plant", ***Advances in Civil Engineering***, Vol. 2018, (2018), 2698319. DOI: 10.1155/2018/2698319.
5. Jiang, W., "Direct Method of Generating Floor Response Spectra", University of Waterloo, Civil and Environmental Engineering, Waterloo, Canada, Doctoral Thesis, (2016),
6. KEPCO and KHNP, *Status Report – APR1400*. 2020, Korea Electric Power Corporation and Korea Hydro & Nuclear Power Co., Ltd. .
7. Hur, J., Wang, Z., Shafieezadeh, A. and Kim, M., "Seismic reliability analysis of NPP's nonstructural components using surrogate models", in 13th International Conference on Applications of Statistics and Probability in Civil Engineering, Seoul, South Korea, (2019).
8. Mondal, G. and Jain, S.K., "Design of non-structural elements for buildings: A review of codal provisions", ***The Indian Concrete Journal***, Vol. 79, (2005), 22-28.
9. Chaudhuri, S.R. and Villaverde, R., "Effect of building nonlinearity on seismic response of nonstructural components: A

parametric study", ***Journal of Structural Engineering***, Vol. 134, No. 4, (2008), 661-670. DOI: 10.1061/(ASCE)0733-9445(2008)134:4(661).

10. Merz, K. and Ibanez, P., "Guidelines for estimation of cabinet dynamic amplification", ***Nuclear Engineering and Design***, Vol. 123, No. 2-3, (1990), 247-255. DOI: 10.1016/0029-5493(90)90244-R.
11. Pardalopoulos, S.I. and Pantazopoulou, S.J., "Seismic response of nonstructural components attached on multistorey buildings", ***Earthquake Engineering & Structural Dynamics***, Vol. 44, No. 1, (2015), 139-158. DOI: 10.1002/eqe.2466.
12. CSI, *Getting Started With SAP2000 (Integrated Solution for Structural Analysis and Design)*. 2018, Computers and Structures, Inc.: Berkeley, CA, USA.75.
13. Kim, B.H., Stubbs, N. and Park, T., "A new method to extract modal parameters using output-only responses", ***Journal of Sound and Vibration***, Vol. 282, No. 1, (2005), 215-230. DOI: 10.1016/j.jsv.2004.02.026.
14. Cara, J., "Modal identification of structures from input/output data using the expectation–maximization algorithm and uncertainty quantification by mean of the bootstrap", ***Structural Control and Health Monitoring***, Vol. 26, No. 1, (2019), e2272. DOI: 10.1002/stc.2272.
15. Park, B.-H. and Kim, K.-J., "Vector ARMAX modeling approach in multi-input modal analysis", ***Mechanical Systems and Signal Processing***, Vol. 3, No. 4, (1989), 373-387. DOI: 10.1016/0888-3270(89)90044-7.
16. Brown, D.L., Allemang, R.J., Zimmerman, R. and Mergeay, M., "Parameter estimation techniques for modal analysis", ***SAE Technical Papers***, Vol. 88, No. 1, (1979), 828-846. DOI: doi.org/10.4271/790221.
17. Huang, W., Pei, M., Liu, X., Yan, C. and Wei, Y., "Nonlinear optimization of orthotropic steel deck system based on response surface methodology", ***Research***, Vol. 2020, (2020), 1303672. DOI: doi.org/10.34133/2020/1303672.
18. Cao, A.-T., Nahar, T.T., Kim, D. and Choi, B., "Earthquake risk assessment of concrete gravity dam by cumulative absolute velocity and response surface methodology", ***Earthquakes and Structures***, Vol. 17, No. 5, (2019), 511-519. DOI: 10.12989/eas.2019.17.5.511.
19. Rastbood, A., Gholipour, Y. and Majdi, A., "Finite element based response surface methodology to optimize segmental tunnel lining", ***Engineering, Technology & Applied Science Research***, Vol. 7, No. 2, (2017), 1504-1514. DOI: 10.48084/etasr.1045.
20. Sadeghifar, M., Sedaghati, R., Jomaa, W. and Songmene, V., "Finite element analysis and response surface method for robust multi-performance optimization of radial turning of hard 300M steel", ***The International Journal of Advanced Manufacturing Technology***, Vol. 94, No. 5, (2018), 2457-2474. DOI: 10.1007/s00170-017-1032-4.
21. Nahar, T.T., Cao, A.-T. and Kim, D., "Risk assessment of aged concrete gravity dam subjected to material deterioration under seismic excitation", ***International Journal of Concrete Structures and Materials***, Vol. 14, No. 1, (2020), 53. DOI: 10.1186/s40069-020-00430-z.
22. Tran, T.-T., Cao, A.-T., Nguyen, T.-H.-X. and Kim, D., "Fragility assessment for electric cabinet in nuclear power plant using response surface methodology", ***Nuclear Engineering and Technology***, Vol. 51, No. 3, (2019), 894-903. DOI: 10.1016/j.net.2018.12.025.
23. Dabiry, Y., Nikoi, R. and dabiry, y., "An Experimental Study on the Tensile Behaviors of Ultrasonic Welded T-joints for Polyamide Composite", ***International Journal of Engineering, Transactions C: Aspects,*** Vol. 29, No. 12, (2016), 1783-1790. DOI: 10.5829/idosi.ije.2016.29.12c.18.
24. Rahman, M.M., Nahar, T.T., Baek, G. and Kim, D., "Seismic response characterization of shear wall in auxiliary building of nuclear power plant", ***Journal of the Earthquake Engineering Society of Korea***, Vol. 25, No. 3, (2021), 93-102. DOI: 10.5000/EESK.2021.25.3.093.
25. Ozturk, B., "Seismic behavior of two monumental buildings in historical Cappadocia region of Turkey", ***Bulletin of Earthquake Engineering***, Vol. 15, No. 7, (2017), 3103-3123. DOI: 10.1007/s10518-016-0082-6.
26. ACI, *Building Code Requirements for Structural Concrete* 2011, American Concrete Institute: Michigan, United States.503.
27. Chopra, A.K., "Dynamics of Structures: Theory and Applications to Earthquake Engineering", 4th ed, Hoboken, NJ, USA, Prentice Hall, (2012), 992.
28. Salman, K., Tran, T.-T. and Kim, D., "Grouping effect on the seismic response of cabinet facility considering primary-secondary structure interaction", ***Nuclear Engineering and Technology***, Vol. 52, No. 6, (2019), 1318-1326. DOI: 10.1016/j.net.2019.11.024.
29. Myers, R.H., Montgomery, D.C. and Anderson-Cook, C.M., "Response Surface Methodology: Process and Product in Optimization using Designed Experiments", 4th ed, Hoboken, NJ, USA, John Wiley & Sons, Inc., (2016), 855.
30. Yousefi, M., Safikhani, H., Jabbari, E., Yousefi, M. and Tahmsbi, V., "Numerical modeling and optimization of respirational emergency drug delivery device using computational fluid dynamics and response surface method", ***International Journal of Engineering, Transactions B: Applications,*** Vol. 34, No. 2, (2021), 547-555. DOI: 10.5829/ije.2021.34.02b.28.
31. Sadhukhan, B., Mondal, N.K. and Chattoraj, S., "Optimisation using central composite design (CCD) and the desirability function for sorption of methylene blue from aqueous solution onto Lemna major", ***Karbala International Journal of Modern Science***, Vol. 2, No. 3, (2016), 145-155. DOI: 10.1016/j.kijoms.2016.03.005.
32. Venkata Vishnu, A. and Sudhakar Babu, S., "Mathematical modeling & multi response optimization for improving machinability of alloy steel using RSM, GRA and Jaya algorithm", ***International Journal of Engineering, Transactions C: Aspects***, Vol. 34, No. 9, (2021), 2157-2166. DOI: 10.5829/ije.2021.34.09C.13.
33. Iffat, S., "Relation between density and compressive strength of hardened concrete", ***Concrete Research Letters***, Vol. 6, No. 4, (2015), 182-189.
34. Grünewald, S. and Walraven, J.C., "Properties of fibre reinforced SCC", in Self-Compacting Concrete: Materials, Properties and Applications, R. Siddique (Ed.), Vol., Woodhead Publishing, Sawston, UK, (2020), 309-370, (Chapter 12). DOI: 10.1016/B978-0-12-817369-5.00012-X.
35. Alin, A., "Minitab", ***Wiley Interdisciplinary Reviews: Computational Statistics***, Vol. 2, No. 6, (2010), 723-727. DOI: 10.1002/wics.113.
36. Kazemian, M.E. and Gandjalikhan Nassab, S.A., "Thermodynamic Analysis and Statistical Investigation of Effective Parameters for Gas Turbine Cycle using the Response Surface Methodology", ***International Journal of Engineering, Transactions B: Applications***, Vol. 33, No. 5, (2020), 894-905. DOI: 10.5829/ije.2020.33.05b.22.
37. Sahu, N.K. and Andhare, A.B., "Multiobjective optimization for improving machinability of Ti-6Al-4V using RSM and advanced algorithms", ***Journal of Computational Design and Engineering***, Vol. 6, No. 1, (2018), 1-12. DOI: 10.1016/j.jcde.2018.04.004.
38. NRC, U.S., *Regulatory Guide 1.60: Design Response Spectra for Seismic Design of Nuclear Power Plants*, in *US NRC*. 2014, United States Nuclear Regulatory Commission.13.

39. AIK, *Korean Building Code-Structural*. 2016, Architectural Institute of Korea: Seoul, Korea.
40. Uniform Building Code™, "Uniform Building Code: Structural Engineering Design Provisions, Whittier, CA, USA, International Conference of Building Officials, Vol. 2, (1997), 503.
41. Kim, D., *Quake_M: Response Spectra Based Earthquake Generation*. 2013, Structural System Laboratory: Cheonan, Korea.
42. Hur, J.S., Abdollah, "Performance of nonstructural components in NPPs under high-frequency ground motions", in 13th International Conference on Applications of Statistics and Probability in Civil Engineering, Seoul, South Korea, (2019).

Persian Abstract

چکیده

برای اطمینان از عملکرد ایمن و پایدار نیروگاه های هسته ای (NPP)، بسیاری از اجزای غیر ساختاری (NSCs) به طور فعال با NPP مرتبط هستند. به طور کلی، برای طراحی NSC ها، از طیف پاسخ طبقه (FRS) استفاده می شود، با این وجود، تمرکز بر موقعیت نصب و فرکانس NSC ها ضروری است که معمولا در طراحی معمولی NSC ها نادیده گرفته شود. این مقاله اثر محل نصب NSCها را در یک طبقه در یک ساختمان کمکی از نوع کانال ارزیابی می‌کند.تخمین پارامتر مودال برای بدست آوردن ویژگی دینامیکی ساختمان کمکی NPP توسط آزمون میز لرزان در نظر گرفته شده است، که منجر به کالیبراسیون FEM می شود. کالیبراسیون FEM از طریق روش سطح پاسخ (RSM) انجام شد و مدل کالیبره شده با استفاده از پارامترهای مدال و همچنین تابع طیف پاسخ فرکانسی تأیید شده است. در نهایت، حساسیت مکان با استفاده از تجزیه و تحلیل تاریخچه زمانی (THA) تحت زلزله‌های سازگار با طیف پاسخ طراحی و حرکات سینوسی به‌طور مصنوعی مورد بررسی قرار گرفت. نتایج نشان می‌دهد که انتخاب مکان مناسب برای NSCها می‌تواند یک اقدام مهم برای کاهش پاسخ‌های نامطلوب در هنگام زلزله باشد که می‌تواند تا ۳۰٪ پاسخ‌های افقی و ۷۰٪ پاسخ های عمودی شتاب دوره صفر (ZPA) را در ساختمان‌های کمکی نوع کانال کاهش دهد.